


Benthic biology influences sedimentation in submarine channel bends: Coupling of biology, sedimentation and flow

M. Azpiroz-Zabala^{1,2,3}  | E. J. Sumner³ | M. J. B. Cartigny⁴ | J. Peakall⁵ |
M. A. Clare¹ | S. E. Darby⁶ | D. R. Parsons⁷ | R. M. Dorrell⁷ | E. Özsoy^{8,9} |
D. Tezcan⁹ | R. B. Wynn³ | J. Johnson⁷

¹National Oceanography Centre of Southampton, Southampton, UK

²Arquimea Research Center, Edif. Nanotec. Parque Urbano Las Mantecas, Santa Cruz de Tenerife, Spain

³School of Ocean and Earth Science, University of Southampton, Southampton, UK

⁴Geography Department, University of Durham, Durham, UK

⁵School of Earth and Environment, University of Leeds, Leeds, UK

⁶School of Geography and Environmental Sciences, University of Southampton, Southampton, UK

⁷Energy and Environment Institute, University of Hull, Hull, UK

⁸Eurasia Institute of Earth Science, İstanbul Technical University, İstanbul, Turkey

⁹Institute of Marine Sciences, Middle East Technical University, Mersin, Turkey

Correspondence

M. Azpiroz-Zabala, National Oceanography Centre of Southampton, European Way, Southampton, Hampshire SO14 3ZH, UK.
Email: emeazeta@gmail.com

Funding information

Natural Environment Research Council, Grant/Award Number: NE/F020120/1, NE/F020279/1 and NE/F020511/1

Abstract

Submarine channels are key features for the transport of flow and nutrients into deep water. Previous studies of their morphology and channel evolution have treated these systems as abiotic, and therefore assume that physical processes are solely responsible for morphological development. Here, a unique dataset is utilised that includes spatial measurements around a channel bend that hosts active sediment gravity flows. The data include flow velocity and density, alongside bed grain size and channel-floor benthic macrofauna. Analysis of these parameters demonstrate that while physical processes control the broadest scale variations in sedimentation around and across the channel, benthic biology plays a critical role in stabilising sediment and trapping fines. This leads to much broader mixed grain sizes than would be expected from purely abiotic sedimentation, and the maintenance of sediment beds in positions where all the sediment should be actively migrating. Given that previous work has also shown that submarine channels can be biological hotspots, then the present study suggests that benthic biology probably plays a key role in channel morphology and evolution, and that these need to be considered both in the modern and when considering examples preserved in the rock record.

KEYWORDS

gravity flow, interplay flow-sediment-biology, subaqueous channel evolution, submarine channel bend

1 | INTRODUCTION

Submarine channels are distinctive large-scale sea floor features that funnel globally important volumes of sediment hundreds of kilometres from the shallow continental shelves into the deep sea (Khripounoff et al., 2003; Peakall & Sumner, 2015). These systems generally evolve from V-shaped canyons incised on the continental shelf (Kuenen, 1953; Wynn et al., 2007; Harris & Whiteway, 2011) to U-shaped channels with overbank deposits (Walker & Mutti, 1973; Clark & Pickering, 1996). Within submarine channels, sediments, nutrients and pollutants are transported by avalanche-like submarine density flows (Talling et al., 2013; Kane & Clare, 2019). Indeed, the presence of nutrients within sediment gravity flows can result in submarine channels being biodiversity hot spots for benthic organisms (Griggs et al., 1969; Olu et al., 2017) that form ecological niches (Sen et al., 2017) associated with the specific morphology of the channel (Pozzato et al., 2017; Sen et al., 2017). This handful of studies on biodiversity in submarine channels is in keeping with knowledge of biodiversity hotspots in the far better studied submarine canyons (Stefanescu et al., 1994; Gili et al., 1999; Paradis et al., 2017).

Submarine channels are typically sinuous (Babonneau et al., 2010), particularly in low latitudes (Peakall et al., 2012). Previous studies have investigated: how bends affect the velocity and density structure of submarine density flows (Kassem & Imran, 2004; Dorrell et al., 2013; Sumner et al., 2014; Azpiroz-Zabala et al., 2017a); the link between sediment distribution and bend geomorphology (Kane et al., 2008; Amos et al., 2010; Fernandes et al., 2020); and the relationship between bends and the distribution of organisms (Pozzato et al., 2017; Sen et al., 2017). However, each of these aspects has been looked at in isolation, and most of the field studies have only measured individual points or transects rather than spatial patterns around a bend (exceptions for flow are: Wei et al., 2013; Sumner et al., 2014). Therefore, no study has investigated the coupling between sediment distribution and flow or examined what role biology may play in influencing sedimentation in submarine channel bends. Consequently, the working assumptions when looking at submarine channel deposits in the rock record are that: (i) flow patterns exclusively drive sedimentation patterns in bends; and (ii) in terms of processes, bends are essentially abiotic.

Here, these gaps in our understanding of submarine channel bends and long-standing assumptions are addressed using a unique dataset that includes measurements of the three-dimensional dynamics of a channelised sea floor sediment gravity flow, along with

sea floor samples that document the spatial distribution of sediment characteristics and benthic organisms. Feedbacks between flow dynamics, sediment distribution and biological organisms are then investigated in the broader context of the bend-scale geomorphology. Based on this analysis, the present paradigm that the role of benthic biology in submarine bends is inconsequential and can be ignored is challenged.

2 | STUDY AREA AND PREVIOUS WORK

The study area is located on the shallow Black Sea shelf, to the north of the Strait of Bosphorus, which connects the Black Sea to the Marmara Sea (Figure 1). The salinity of the Mediterranean water is *ca* 12 to 16 psu (practical salinity units) higher than the Black Sea water. This difference in salinity results in a sea floor density current comprising Mediterranean water that enters the Black Sea (Flood et al., 2009). The study area contains a channel that has most probably hosted sea floor density flows for the past *ca* 8 cal kyr, following a robust connection between the Mediterranean Sea and the Black Sea through the Strait of Bosphorus (Aksu & Hiscott, 2022). The study area has water depths ranging from 40 to 85 m, while the channel itself is *ca* 35 m deep with widths of between 400 and 725 m. Within the channel, the sea floor density current achieves speeds of up to 1.2 m/s and is quasi-continuous, with exceptions on daily to interannual timescales (Ünlülata et al., 1990; Gregg & Özsoy, 1999; Gregg et al., 1999; Özsoy et al., 2001). This flow speed is sufficient to transport sea floor sediment as bedload and to develop the channel system, which displays coarse-grained bedforms in the channel and fine-grained sediment waves on the overbanks (Figure 1; Flood et al., 2009).

The study area includes a channel bend that turns counter-clockwise towards the west (Figure 1). This bend is approximately 5 km to the north of the mouth of the Strait of Bosphorus and is 70 to 80 m water depth. Previous studies have surveyed the area to analyse the links between the saline density flow and the sedimentary structures in the area (Flood et al., 2009; Hiscott et al., 2013). Flood et al. (2009) identified local lateral accretion of bars within the channel bend and other sedimentary products and related them to the flow. Hiscott et al. (2013) linked the proposed overspill of the saline flow to sediment waves in overbank regions of the study area and also interpreted seismic data to propose that at the exit of the channel bend, the sea floor comprises bedrock, which probably limits bend erosion and may influence channel geomorphology. Parsons et al. (2010) and Sumner et al. (2013) also studied this saline flow as an analogue to

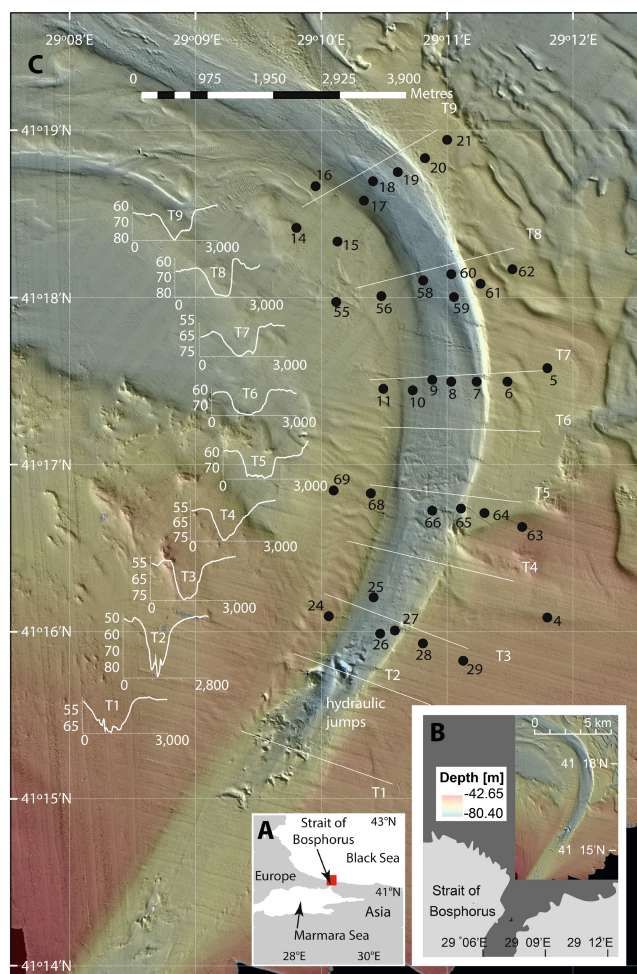


FIGURE 1 Study area. (A) Location of the Strait of Bosphorus in relation to the Black Sea and Marmara Sea. The red square indicates the location of the zoomed-in area in panel B. (B) Location of the submarine bend downstream of the Strait of Bosphorus. (C) Bathymetry of the submarine bend, also showing the locations of the nine transects (T1–T9) used in the analysis. Black dots and numbers indicate the position of the grab sample stations. Cross-channel profiles of each transect are shown on the left of the bend.

turbidity currents; the excess density of this saline density current ($\text{ca } 10\text{--}15 \text{ kg/m}^3$) is comparable to the density contrast of some sediment-laden turbidity currents (Pirmez & Imran, 2003; Konsoer et al., 2013; Azpiroz-Zabala et al., 2017b; Simmons et al., 2020). Parsons et al. (2010) and Sumner et al. (2013) compared the dynamics of the saline flow and rivers, and concluded that radial forces within the flow might be key to determine the direction of the cross-channel velocity component of the saline flow. Previous studies have also identified hydraulic jumps just upstream from the bend (Figure 1); these hydraulic jumps disrupt the flow velocity structure, but the flow stabilises before entering the bend studied here (Sumner et al., 2013; Dorrell et al., 2016).

3 | METHODS

3.1 | Data collection

Data were collected during two oceanographic field seasons, with cruises on board the *RV Koca Piri Reis* in 2010, and a combined campaign with the *RV Pelagia* and *RV Bilim* in 2013. In 2010, 35 sediment grab samples were collected on the 19th and 22nd of May from stations located on the channel thalweg and overbank area (Figure 1). The shipboard descriptions included information about the organisms (alive or fragmented) present in the samples. In 2013, bathymetry data, flow measurements and conductivity temperature depth (CTD) probes were collected from the 28th of June to the 1st of July.

Bathymetric data were collected by a hull-mounted EM302 multibeam echosounder operated at 30 kHz to survey the sea floor, and a Reson SeaBat 7125 system used a 200/400 kHz frequency, which was on an over-the-side pole mount. Vessel position and motion data were captured with an Applanix POS-MV system 320.

Flow velocity was measured using a 600 kHz acoustic Doppler current profiler (ADCP) mounted on the *Autosub3* autonomous underwater vehicle (AUV). The ADCP recorded the velocity of the channelised flow along nine cross-stream transects (T1–T9) aligned perpendicular to, and distributed around, the submarine channel bend (Figures 2, 3 and 4). Each of the nine cross-stream transects was surveyed between two and four times to enable reduction of the measurement scatter from one transect survey and to obtain quantitative details of the flow structure (Szupiany et al., 2007; Parsons et al., 2013). The ADCP bin size was set at 1 m, and the instrument was flown between $\text{ca } 10$ and 40 m above the channel floor, which resulted in the loss of the measurements immediately, 1 to 3 m above the sea floor, due to sea floor acoustic reflection (see Supplementary Information).

The CTD data were collected every 0.25 s over transects T2 through T9. The CTDs on T7 and T8 were surveyed several times (in several days), while the CTDs on the rest of the transects were collected only once.

3.2 | Data processing

3.2.1 | Processing of sediment samples

Grab sediment samples were successfully collected at 35 stations. Most stations were located in close proximity to one of the cross-channel transects (Figure 1). When sample stations were not located on transects, samples were assumed to have been collected from the nearest point located on a transect (maximum distance from station 59 in the bend channel to the transect is $\text{ca } 200 \text{ m}$; see Figure 5).

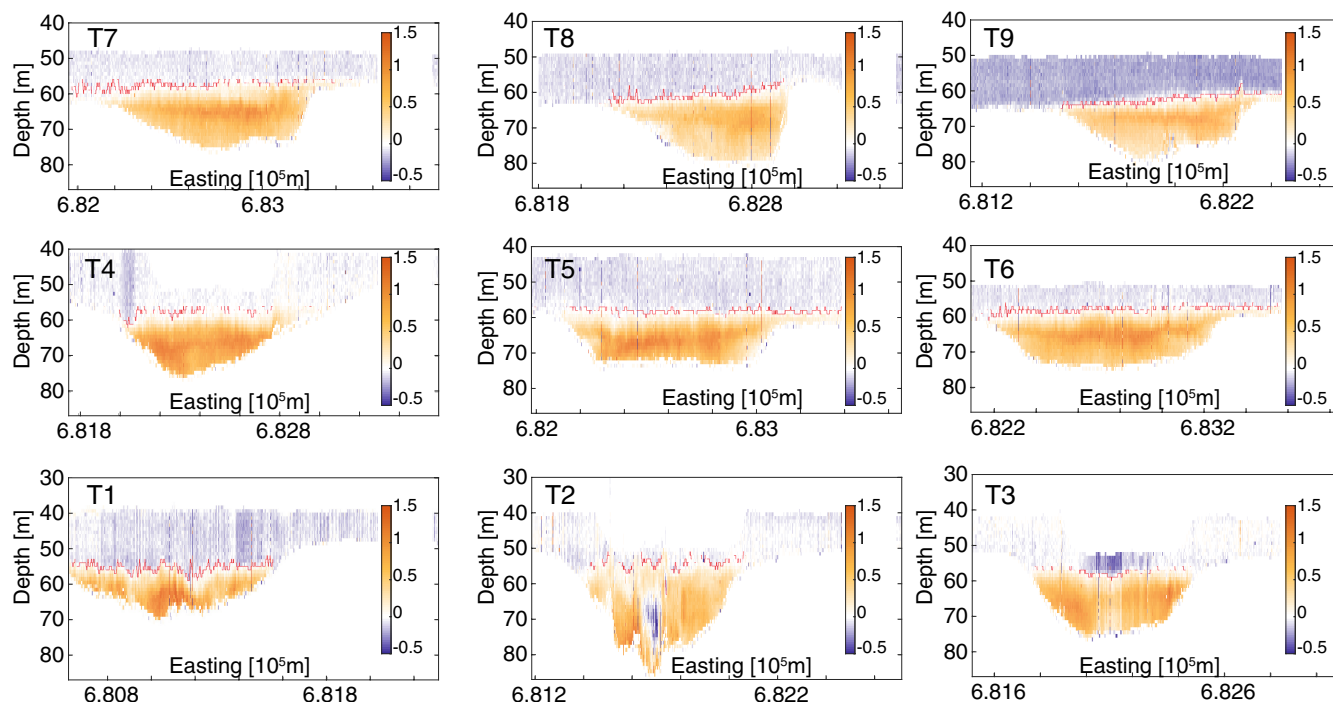


FIGURE 2 Downstream velocity measurements collected by the ADCP over transects T1–T9. Red lines indicate the zero downstream velocity that separates the body of the saline flow from the ambient fluid. Note that the high velocity cores occupy the near-bed (ca 10 m above the bed) zone in transects T1 and T3–T5, but the high velocity core then thins and elevates in transects T6–T9. The flow velocity structure is disturbed in transect T2, which is located immediately downstream of the hydraulic jump area shown in Figure 1. All views show flow into the page; velocity scale in m/s with red/orange colours showing downstream flow and blue colours upstream-directed flow.

The grain-size analysis included both biotic (comprising any macrofauna within shells as well as shell fragments) and abiotic components, following previous work on modern mixed siliciclastic–carbonate systems (Halfar et al., 2004; Brandon & Civitelli, 2007). The sediment samples were processed at the University of Southampton via wet-sieving at half-phi intervals from 11,200 μm down to 63 μm , with the remainder <63 μm recorded. The size distribution of the finest (<63 μm) fractions was determined using a Micromeritics Saturn DigiSizer II digital particle size analyser, but solely utilised here to confirm that clay is present within the samples. The size of the sediment grains ranged from medium sand to clay, and the sample content was categorised as one of these three main fractions: gravel, sand and mud. Clay content was included within the mud fraction. Additionally, d_{10} , d_{50} and d_{90} were obtained using GRADISTAT software, and grain-size distribution curves were drawn for each sample based on the sieved sample data (Figure S1).

3.2.2 | Processing of multibeam data

Multibeam data were processed using CARIS HIPS 8.2. The collected data were subjected to POS-MV PosPac correction using local GPS beacon data to derive a processed

positional solution with a 3D accuracy of 0.06 m, which was also used for vertical tidal corrections. The line data were sound corrected using profiles obtained across the survey areas, including those taken along the transects. Finally, the 3D point clouds were manually filtered to remove spurious mid-water and side lobe interference soundings, resulting in the removal of 1.8% of the data points. The final point cloud data were binned into 10 \times 10 m and 2 \times 2 m grids based on the resolution of the data collected by the EM302 multibeam echosounder and the Reson SeaBat 7125 system, respectively, with the range resolution of the EM302 echosounder being 0.14 m and the range resolution of the Reson SeaBat 7125 being 0.01 cm.

3.2.3 | Processing of flow velocity data

The ADCP data were processed using the following steps implemented in Matlab®:

1. Interpolation of datasets recorded at different time intervals onto a common time interval.
2. Interpolation of bottom track velocity, where data are missing.
3. Removal of AUV velocity component from the ADCP velocity measurements.

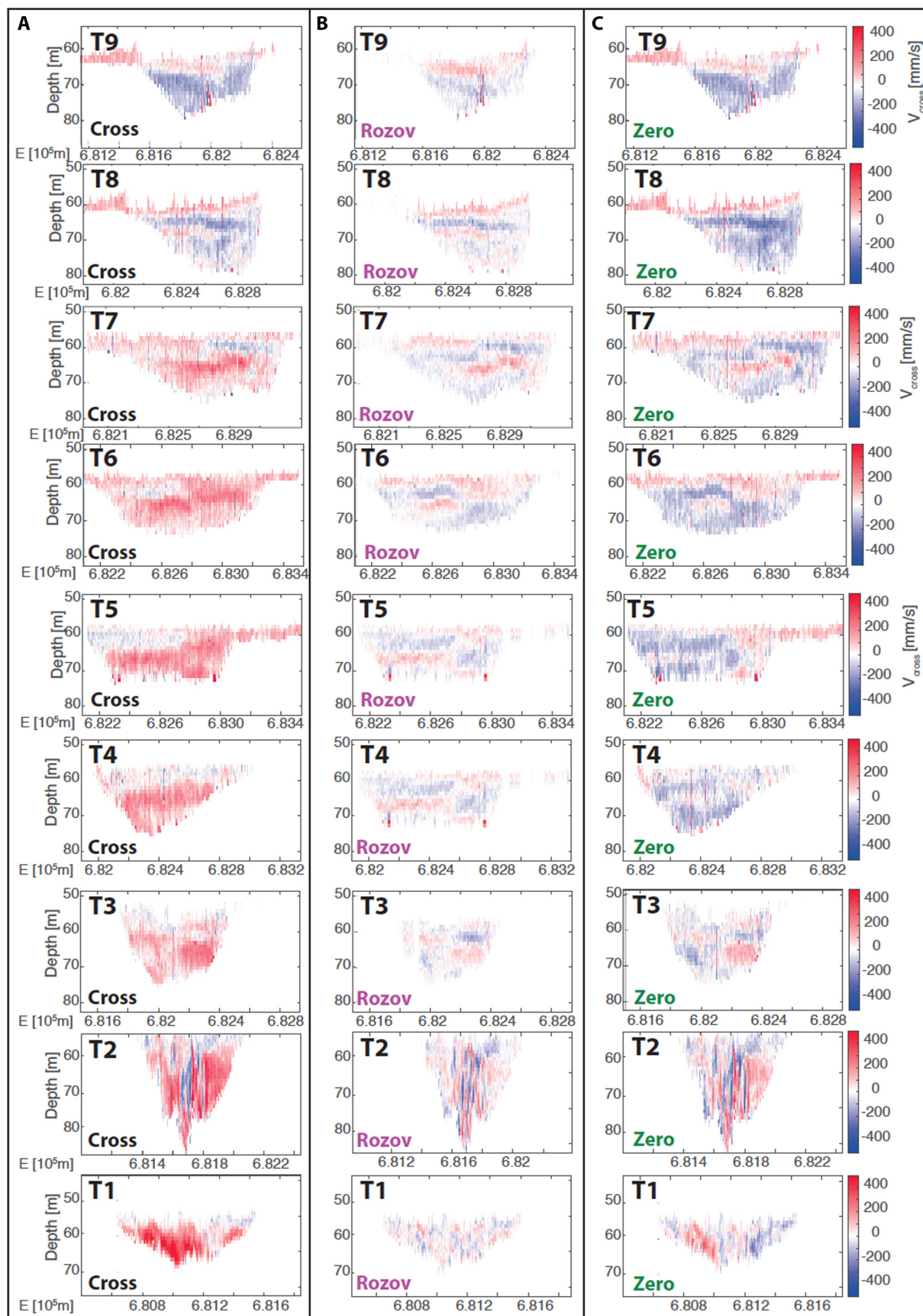


FIGURE 3 Cross-stream velocities based on (A) cross-channel, (B) Rozovskii and (C) whole section direction coordinate systems. Red colours (positive velocities) indicate that the flow is directed towards the outer bend, whereas blue colours (negative velocities) indicate the flow is directed towards the inner bend. All views show flow into the page.

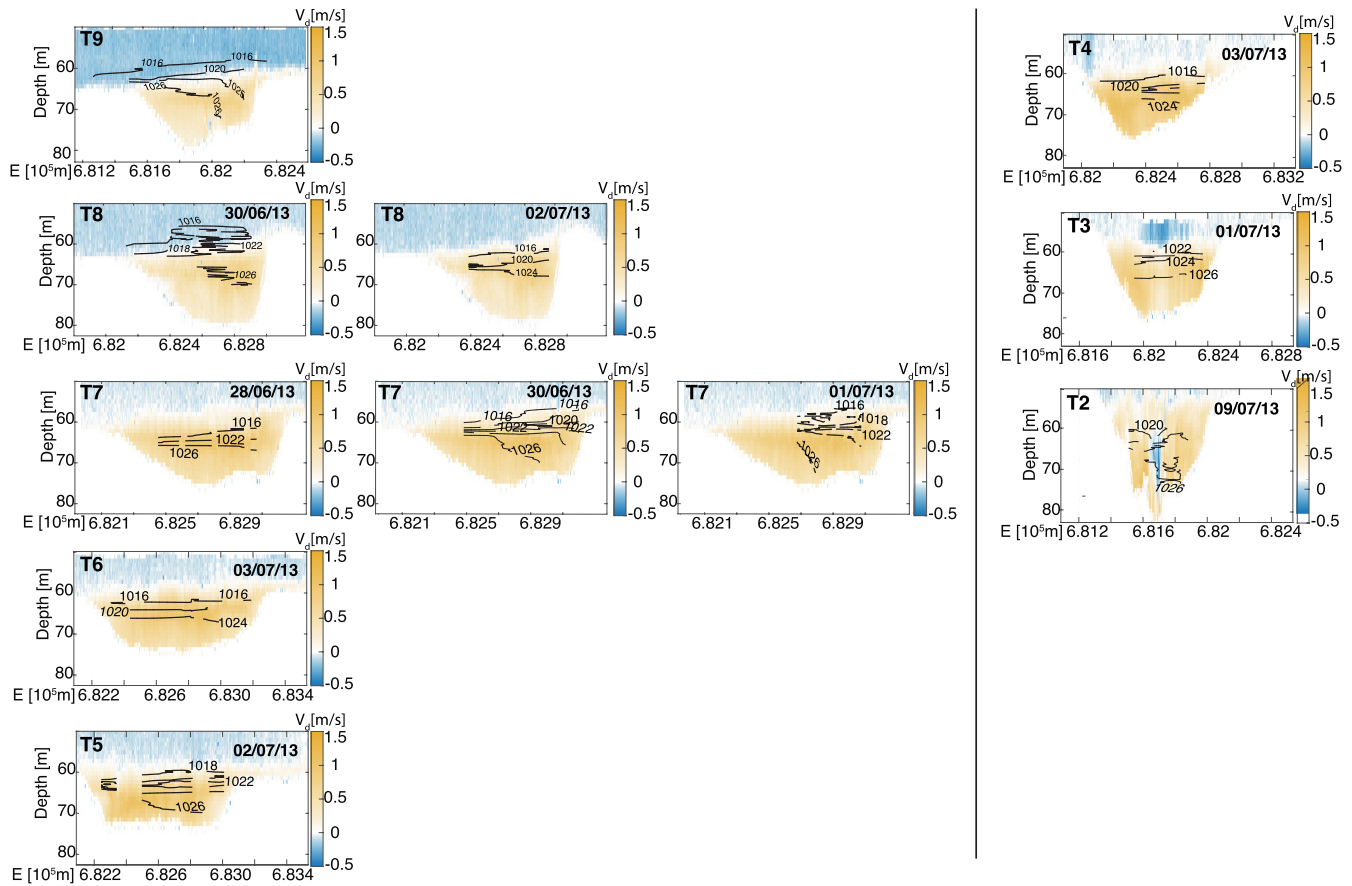


FIGURE 4 Flow density contours superimposed on downstream velocity. The date of CTD acquisition is shown on each panel. The locations of each transect are indicated in Figure 1. All views show flow into the page.

4. Correction of the ADCP deployment setting of East and North velocities relative to the AUV coordinate system (North was originally set as perpendicular to the AUV direction and East as parallel to the AUV direction).
5. Rotation of resultant flow velocities from a coordinate system relative to the AUV to a global coordinate system.
6. Calculation of the depth of each measurement using the height that the AUV was flying above the sea floor and the depth of the AUV beneath the sea surface.
7. Calculation of average straight-line plane (Parsons et al., 2013) for transects T1–T9 that were each surveyed several times (Figure 1).
8. Projection of measurements collected along irregular AUV tracks onto straight-line planes defined in step 7 (Parsons et al. 2013).
9. Interpolation of results on straight-line planes to obtain equally spaced flow measurements.
10. Arrangement of results in terms of UTM Easting coordinate for transects T1–T9.
11. Location of the top of the saline flow at each transect where the velocity perpendicular to the transect is zero (Figure 2).
12. Extraction of the saline flow velocities parallel and perpendicular to the transects T1–T9.
13. Calculation of the ADCP side lobe interference area (SLIA) from the measured elevation of the ADCP over the seabed and the 20° ADCP beam angle to the vertical (Figure S2).
14. Substitution of measurements of velocities in ADCP SLIA with linearly interpolated values to zero at bed level.

These steps then provide 3D velocity data along nine cross-channel transects.

3.3 | Two-dimensional and 3D representations of flow velocity

The north, east and vertical components of the measured velocities calculated in processing step five define the 3D flow velocity. The secondary flow for each transect was calculated. Effectively, secondary flow is a 2D representation of the across channel portion of the 3D flow field. The calculation of this enables the results to be compared with

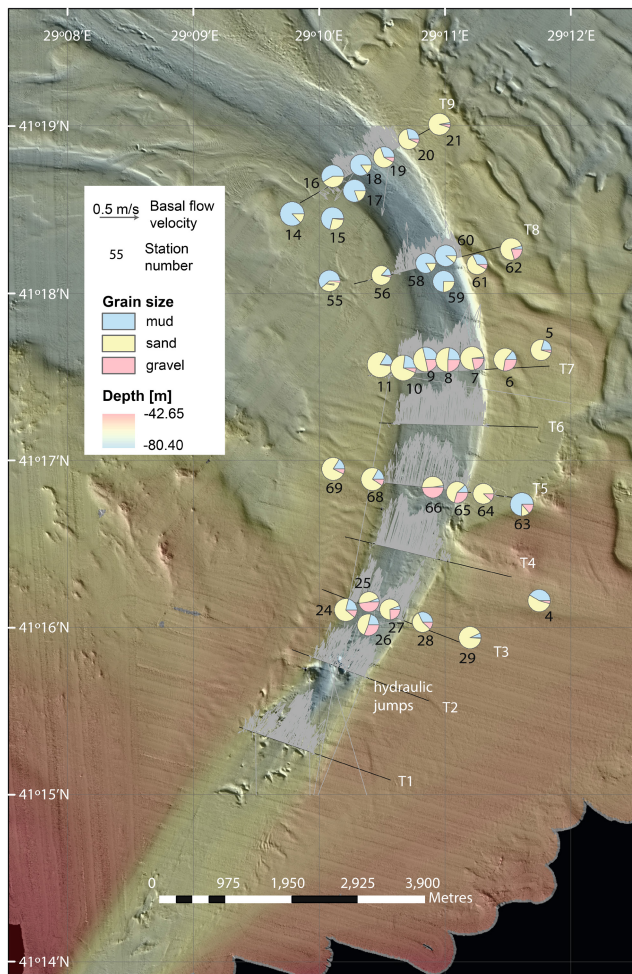


FIGURE 5 Near-bed flow velocities in relation to bed material size. Grey arrows represent the three-dimensional flow velocity at a height of 3 m over the sea floor ($Z/H \sim 0.1$). Black numbers represent grab sample station.

other studies that did not measure the full 3D flow field. There are three methods that can be used to calculate secondary flow according to how the primary flow direction is defined. (1) ‘cross-channel’, in which the primary flow is assumed to be parallel to the channel orientation (called ‘Cross’ in Figure 3); (2) ‘Rozovskii’, in which the primary flow is determined as the dominant mean flow within each individual velocity profile (called ‘Rozov’ in Figure 3); and (3) zero net flow in the cross-stream section or ‘zero net flow’, in which the primary flow is taken in such a way that it aligns with the dominant mean flow of the whole transect (called ‘Zero’ in Figure 3; see the Supplementary Information section for further explanation).

3.4 | Near-bed flow velocity

Near-bed flow velocity in this work corresponds to the 3D flow velocity at a height of 3 m above the base of the

measured velocity depth profile, that is 0.1 to 0.2 of the total flow depth. Measurements below 3 m of height are recorded by the ADCP but were contaminated in some profiles by sea floor acoustic interference. As 3 m is the common height for all profiles where non-contaminated records were collected, any measurement below that depth has not been considered (see Supplementary Information, Figure 5 and S2). In order to correlate the near-bed flow velocities to the grab samples and due to the spatial resolution in data collection being different, the closest 100 flow velocity measurements to each grab sample were averaged, which represents a horizontal distance of *ca* 16 m.

3.5 | Shear velocity (u^*)

The shear velocity at each measured depth was calculated following the law of the wall that assumes that the shear velocity relates to the gradient of the logarithmic vertical profile of the flow velocity. The law of the wall is expressed as:

$$\frac{u}{u^*} = \frac{1}{\kappa} \ln \left(\frac{z}{z_0} \right) \quad (1)$$

Here, u is the velocity at an elevation z over the seabed, κ is von Karman's constant (assumed here to take a value of 0.405) and z_0 is the height at which u is zero.

Using the least squares regression method by Yu and Tan (2006), u^* was calculated as:

$$u^* = \kappa \frac{n \sum u_i \ln z_i - \sum u_i \sum \ln z_i}{n \sum \ln^2 z_i - (\sum \ln z_i)^2} \quad (2)$$

where n is the number of data points used for the least squares regression, with a minimum of three points below the peak flow velocity height (n is between 19 and 30 depending on the station) used in the computations. This restriction implies that u^* was only calculated for vertical profiles of flow velocity with at least three measurements between the maximum flow velocity and the first measurement above the acoustically contaminated side lobe interference area (SLIA), the size of which varies among different velocity profiles (Supplementary information; Figures 6 and S2).

Each sediment sample was associated with an average shear velocity, calculated by taking the average of the closest 100 shear velocity measurements to the sample station (100 profiles cover *ca* 16 m of transect). This averaged shear velocity was used to estimate the potential for sediment mobilisation using a mobility diagram (de Leeuw et al., 2016) that compares the Reynolds particle number Re_p (ratio between inertial and gravitational forces over sediment grains) and the Shields parameter τ (ratio between frictional and gravity forces).

3.5.1 | Processing of density data

The CTD measurements were processed according to the following procedure:

1. Application of the UNESCO, 1983 methodology to obtain flow density profiles from the conductivity, temperature and depth CTD measurements (UNESCO, 1983).
2. CTD profiles were collected at several stations along cross-stream transects T2–T9 (Figure 1). Data at the same depth between stations were linearly interpolated in Matlab®.

3. Arrangement of results in terms of Easting.

4. CTD profiles collected along transects T7 and T8 were collected on different days. The above procedure was followed for the measurements collected on each day.

4 | RESULTS

In this section, the saline density current flow is first characterised in terms of its flow density and velocity in order to estimate how the flow transports sediment as bedload and

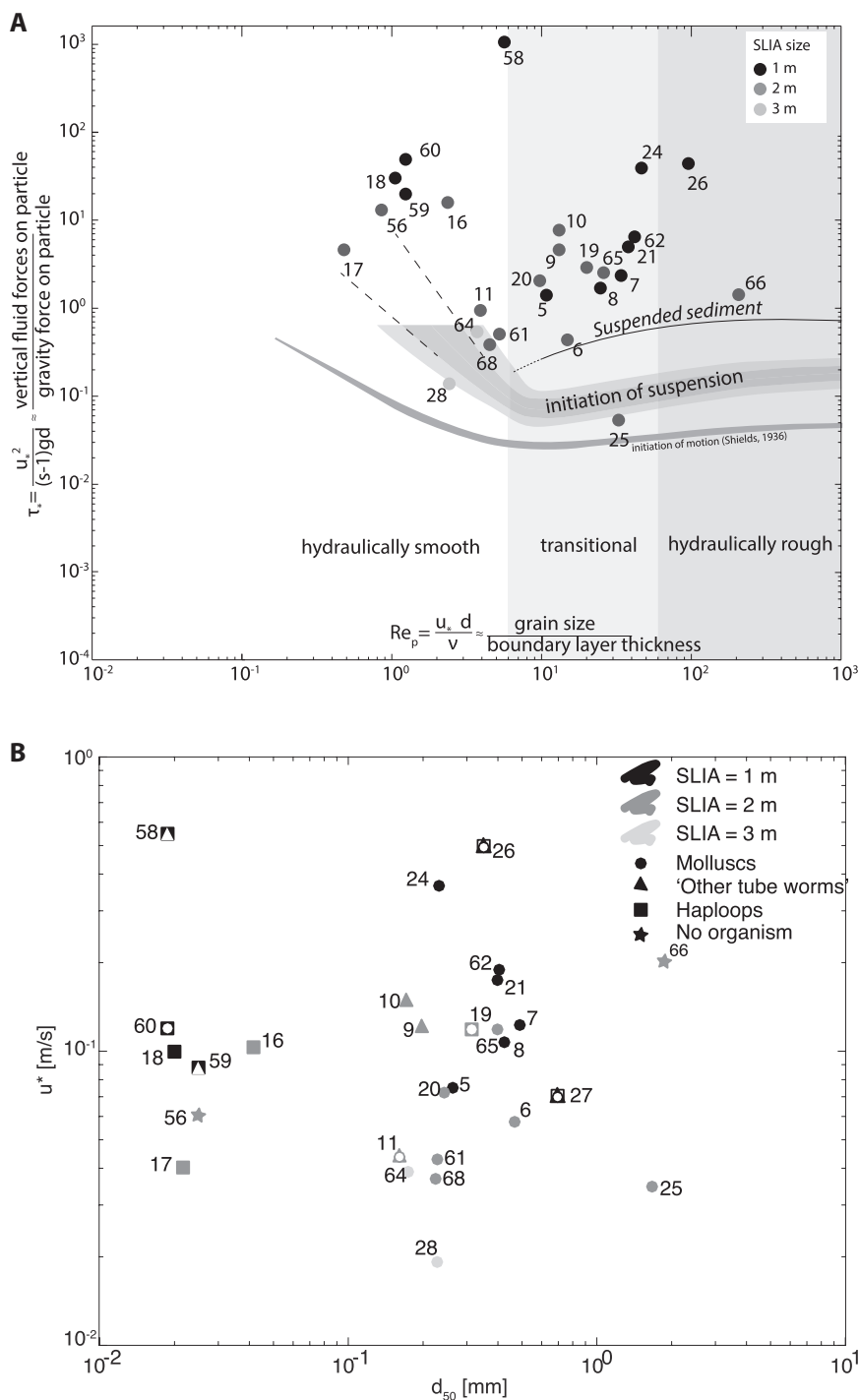


FIGURE 6 Mobility diagram and correlation between average shear velocity (u^*) and median bed-material diameter (d_{50}). (A) Mobility diagram (modified from de Leeuw et al., 2016) predicting sediment transport either as bedload or suspended sediment. Based on d_{50} , most of the sediment collected in the study area is predicted to be transported in suspension at the measured flow velocities. Numbers indicate sample station. Dot colours (black, dark grey and pale grey) indicate the size of the side lobe interference area for each measurement. (B) Correlation between averaged u^* and sediment grain size (d_{50}) across a range of velocity and varying biology. Samples with more than one type of organism are identified with two or three overlapping biological symbols. Numbers indicate grab sample station.

controls sea floor sediment distribution around the bend. For this reason, the near-bed part of the flow and the sediment fractions collected in the grab samples are described. Then, the biological content of the samples is described, and sediment mobility in relation to calculated flow shear velocities is analysed. Finally, a summary and integration of the results in each section are provided.

4.1 | Flow characterisation

The density structure of the saline flow is similar in all transects apart from T2, which is affected by hydraulic jumps (Figure 4). The maximum and minimum density values of the saline density flow are 1027 and 1016 g/L, respectively. The maximum density gradient within the same cross-section occurs at the bend apex (T7). There, the minimum vertical distance between the maximum and minimum density values (*ca* 3 m) is found in the inner part of the bend (Figure 4). The minimum density gradient occurs *ca* 4 km upstream of the bend (at transect T3), where the vertical distance between isopycnals 1027 and 1016 g/L reaches *ca* 10 m. The flow is not strongly stratified, although the densest fluid visibly accumulates in the inner bend (Figure 4), as previously observed in other saline flows, downstream of transect T5 (Sumner et al., 2014). The collection of multiple CTD casts on different days in transects T7 and T8 enables the analysis of density variability on different days. In transect T7, the 1024 g/L isopycnal rises 5 m between the 28th and the 30th June, although the density at the sea floor of 1027 g/L remains constant (Figure 4). A similar *ca* 1027 g/L density is observed on the 30th June at the sea floor in the inner bend of transect T8. This value decreases to 1025 g/L by the 2nd July (Figure 3). The density fields are coupled to the velocity field, with each feeding back into the other (Sumner et al., 2013; Wells & Dorrell, 2021).

The ADCP data reveal that the downstream flow has velocities of up to 1.5 m/s in the proximal transects of the submarine channel system (T1–T7) overlain by the ambient fluid of the Black Sea that moves in the opposite direction with velocities of up to 0.5 m/s (Figures 1 and 4). Across-stream flow velocities vary from maximum values of *ca* 0.4 to 0.1 m/s, depending on the method of calculation (Figure 3). The calculation of the 2D cross-stream flow using the ‘cross-channel’, ‘Rozovskii’ and ‘zero net flow’ methods show large differences (Figures 3 and S3). These differences support previous work on helical flow around bends that highlight the importance of characterising the flow in 3D rather than 2D (Dorrell et al., 2013; Sumner et al., 2013; Peakall & Sumner, 2015; Azpiroz-Zabala et al., 2017a).

The direction and magnitude of the near-bed flow influence sea floor sediment transport and, hence, sediment

distribution around the bend. In proximal transects of the channel (T1–T3), this flow structure changes in both magnitude and direction either at or downstream of the hydraulic jumps identified in the channel bend (Figure 5). Upstream of the bend apex (transects T4–T7), near-bed velocity vectors (3 m above the base; *ca* 10% of the flow depth) show similar magnitudes among transects and within the same transect, where velocity maintains a relatively uniform direction across the whole cross-section of the channel. In these transects, velocity vectors are strongly outwardly directed (towards outer bank) with velocities of up to *ca* 0.7 m/s (Figure 5). Downstream of the bend apex (transects T8 and T9), near-bed velocity vectors show reduced magnitudes (up to *ca* 0.3 m/s) compared to velocity vectors upstream of the bend apex. In these transects, velocity also remains uniform within the channel bend, displaying an outward direction (Figure 5). Upstream-directed low near-bed flow velocities (*ca* 0.1 m/s) were measured in the inner bend of both T8 and T9 transects (Figure 5).

4.2 | Geomorphology and sediment distribution

Two sediment bars are recognisable on the inner and outer banks of the channel bend (Figures 1 and 7; Animation S1). An inner bank bar is located just downstream of the bend apex, whereas an outer-bank bar is located at the exit of the outer bend. An additional sedimentary deposit that forms a nested mound (as defined in Phillips, 1987) occurs upstream of the bend apex on the outer bank of transect T7.

Analysis of the sediment samples within the channel shows that coarse sediment ($d_{50} > 100 \mu\text{m}$) is the most abundant sediment type in the proximal transects (upstream of the bend apex), whereas fine sediment ($d_{50} < 100 \mu\text{m}$) dominates transects located further downstream (Figures 5, 6 and S1).

On a broad scale, sediment type (i.e. gravel, sand and mud) correlates with near-bed flow velocity. Thus, larger sediment sizes occur where near-bed velocities are higher (Figure 5). However, Figure 6 shows a decoupling between measured median grain size (d_{50}) and the flow shear velocity, which mainly oscillates between 0.04 and 0.2 m/s over the whole range of median grain sizes (Figure 6). When plotted on a sediment mobility diagram (Figure 6), sediment at all sample sites (characterised by d_{50}) should be mobile as either bedload or suspension load.

The grain size shows a broad distribution in the samples collected around the bend. The highest size frequency found in each sample corresponds to values that oscillate from <63 to $11,200 \mu\text{m}$ (Figure S1). Some samples (especially muddy samples downstream of the bend apex) show

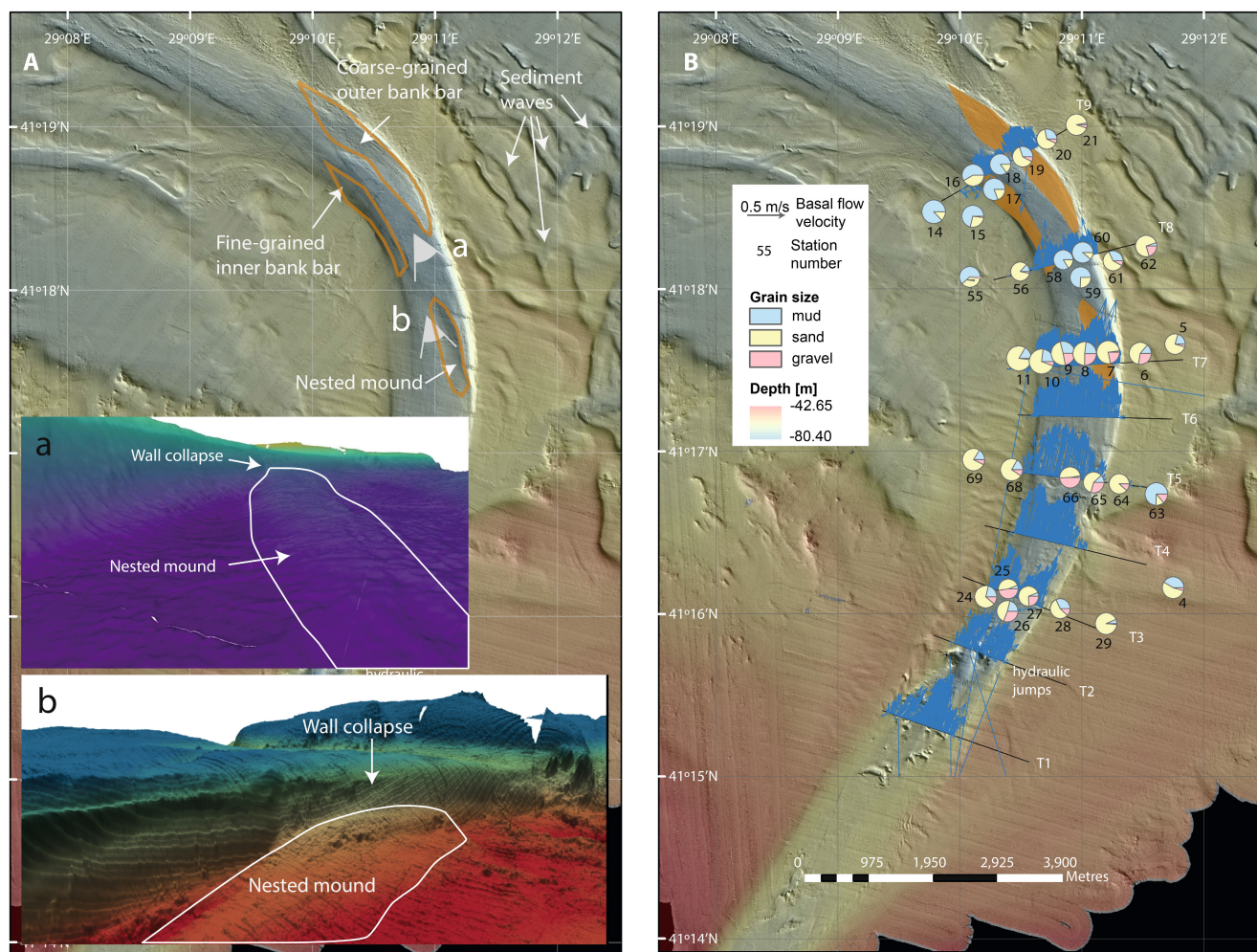


FIGURE 7 (A) Interpretation of sedimentary structures around the bend. Eyes indicate the view of the 3D panel in insets a and b. (a) Detailed view of the submarine channel bend along the direction indicated by the arrow in A. (b) Detailed view of collapsed material from the channel wall. View as indicated by the arrow in A. (B) Overlay of cross-sections, sedimentary structures, near-bed flow velocity and sediment fraction distribution to identify potential links among them. The channel view in the insets in (a) and (b) is extracted from the Animation S1.

good sorting, with 60 to 80% of the sediment composed of the same grain-size category. Approximately half of the samples contain sediment with two dominant grain sizes (over 15% for each size). In most of these cases, the dominant grain sizes are $<63\mu\text{m}$ and 300 to $600\mu\text{m}$, and the samples were mainly collected from the overbanks and downstream of the hydraulic jumps (Figure S1). Samples upstream of the bend apex generally show a wide range of sediment grain-size distribution (Figure S1).

4.3 | Benthic fauna distribution

All but two sediment grab samples were dominated by life (Figure 6). Two groups of animals were predominant in these grab sediment samples: hard-bodied molluscs and soft-bodied organisms living in tubes, of which two species

were found. One of the tube-living species was identified as *haploops* (a type of tube-living amphipod), while the second species could not be characterised (Figure 8). The high density of molluscs was indicated by large amounts of sampled bivalve shells, both complete and fragmented. In the case of the tube-living organisms, their high population density (pervasive throughout the sample beds) was evident by the abundant mineral tubes in the samples, which might be formed by secretions from the animals (Figure 8). Overall, samples collected in areas upstream of the bend apex (T3, T5 and T7), in which gravel and sands were predominantly found, were rich in hard bivalve shells. In contrast, samples from transects at the bend exit, which were basically muddy samples, mainly contained tubes from soft-bodied organisms. The bend apex represented a biological transitional zone. Here, hard-bodied and soft-bodied animals locally cohabited at both the inner and outer bends (Figure 8). Beyond

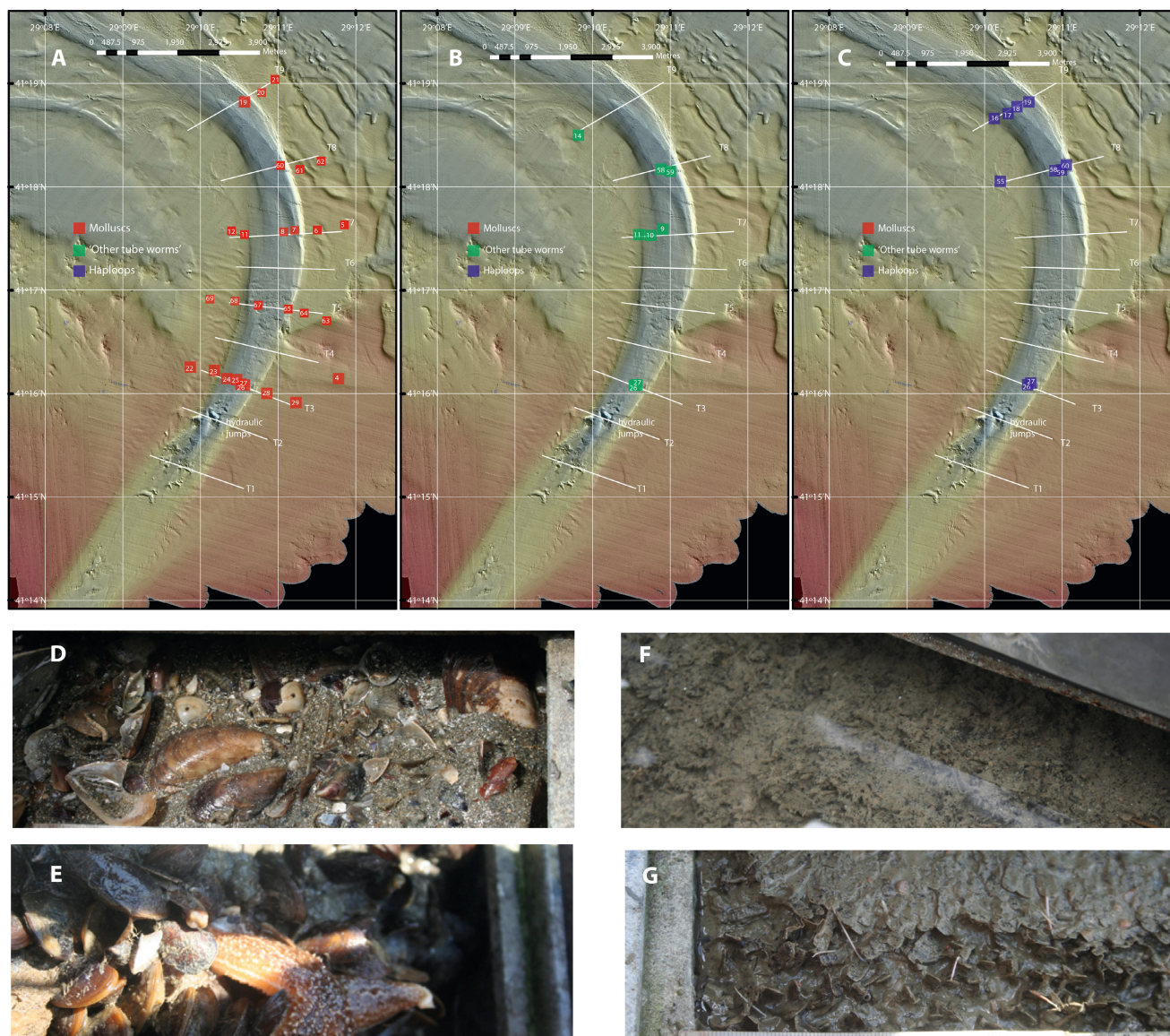


FIGURE 8 Distribution of (A) shells from molluscs, (B) unidentified organisms living in tubes and (C) organisms living in tubes identified as haploids in the study area. The numbers indicate the grab sample station. (D)–(G) Photographs of sediment grabs. (D) and (E) are hard-bodied organisms. (F) Soft-bodied organisms not identified. (G) Soft-bodied organisms identified as haploids. Samples from stations in (A) are shown in (D) and (E), samples from stations in (B) are shown in (F) and samples from stations in (C) are shown in (G).

the bend apex, co-habitation was also observed, but inner bank areas were dominated by *haploids* and other tube-living organisms, while overbank areas on the outer bend were characterised by molluscs.

4.4 | Summary

As a summary of key results:

- There is good spatial agreement between near-bed flow velocity and broad measures of sediment type, that is mud, sand and gravel (Figure 5).
- Despite these broad trends in sediment type, there is not an obvious correlation between near-bed flow velocity/bed shear stress and the median (d_{50}) grain size.
- The distribution of different organisms within the channel appears to correlate with the distribution of different sediment types.

The agreement between near-bed flow, broad sediment type and organism distribution, and the lack of correlation between flow velocity and absolute sediment size (d_{50}) suggests that sediment distribution around this bend does not depend exclusively on the velocity of the saline density flow. Other factors, such as geomorphology,

sediment availability and the distribution of the benthic fauna itself, may play important roles in the sea floor sediment distribution.

5 | DISCUSSION

5.1 | Feedbacks among spatial sediment distribution, flow dynamics, geomorphology and benthic biology

First, the feedbacks between the saline flow dynamics around the submarine bend and sediment transport are discussed. Specifically, the near-bed flow is focussed on and related to the sea floor sediment distribution around the channel bend.

Flows around channel bends have a helical structure, which influences how sediment is transported and deposited by the flow (Dorrell et al., 2013; Sumner et al., 2013). There has been much controversy in recent years regarding the structure of density flows as they travel around channel bends (Bolla Pittaluga & Imran, 2014; Peakall et al., 2014). Much of the controversy about flow structure has resulted from viewing velocity in 2D cross-sections of 3D flows (Figure S2; Dorrell et al., 2013; Sumner et al., 2013; Peakall & Sumner, 2015; Azpiroz-Zabala et al., 2017a). For completeness and to allow comparison with other studies, these calculated secondary flow fields are shown in the results section (Figure 3). However, this study focusses on how sediment is moved around the channel sea floor by the flow as bedload. Therefore, in the remainder of this paper, directly measured 3D near-bed velocities are used (Figure 5) rather than calculated 2D cross-section flow velocities (Figure 3) to explain the channel sediment distribution. Then the feedbacks among sediment type and size, near-bed flow velocity, geomorphology and benthic biology are considered to understand their relative importance.

5.1.1 | Flow velocity, sediment type and geomorphology

There is good spatial agreement between near-bed flow velocity and sediment type, that is gravel, sand and mud (Figure 5). At the bend apex, near-bed flow velocity vectors are outwardly directed revealing the near-bed flow is pushing sediment towards the outer bank to form the observed coarse sediment outer-bank bar and associated overbank sediment waves reflecting overspill (Figure 5; Hiscott et al., 2013). At the inner bank, there is a low-velocity zone with some evidence for flow separation indicated by upstream-directed near-bed flow velocity vectors (transects T8–T9); this zone

correlates with fine sediment deposits (Figure 5). Within the channel, there is a nested mound that appears to result from the reworking of an outer bank wall collapse (Figure 7, Animation S1). The bars and nested mound modify the cross-section channel area, which in turn impacts the near-bed flow velocity distribution (Figure 7). Thus, the flow is partly steered by the bars and also accelerates and decelerates in response to changes in local gradient and confinement caused by the bars. The overall geomorphology of this channel, with bars on both the inner and outer bends, is different from rivers that typically display a well-developed point bar at the inner bank and erosion at the outer bank of the bend (Kolla et al., 2007).

5.1.2 | Flow velocity and sediment size (d_{50}) and distribution

Despite the flow being responsible for sediment transport, there is no obvious correlation between near-bed flow velocity (as represented by the bed shear velocity) and median (d_{50}) grain size (Figure 6B). Furthermore, based on the Shields's diagram, at the calculated shear velocities, the measured bed-material sediment sizes should all be moving rather than being dominantly associated with stable substrates covered in biological organisms (Figure 6A). The Shields diagram does not incorporate the full grain-size distribution, being restricted to the median (d_{50}) diameter. However, the effects of polydispersity are unlikely to change this prediction that bed material should be moving, with the possible exception of the two samples closest to the Shields curve (Figure 6B; Dorrell et al., 2018). Several physical mechanisms may partly explain the observed relationship. The larger grains may form an armouring layer, and thus the d_{50} may be a poor reflection of this coarser bed layer (Ockelford et al., 2020). However, the sediment grain-size distributions are very broad, including high particle contents in the silts and finer classes (Figure S1), suggesting the particles have not accumulated via progressive armouring. This was also reflected in the grab samples, which visually had a high proportion of fines in the top layers. The aforementioned wide sediment grain distributions within samples could, however, be a control, with the high fines content indicating poor sorting and the probable presence of cohesive material alongside the non-cohesive sediment (Figures 5 and S1).

The inability of this flow to segregate sands and larger from finer silts and clays is a key difference from typical rivers, which act as effective size segregators (Frey et al., 2020). Two factors might explain this inefficient cohesivity segregation. First, salinity can play a complex role in clay rheology and cohesion, and might increase

clay shear strength relative to clay in fresh water (Mietta et al., 2009). Second, biological activity and material such as extracellular polymeric substances (EPS), that trap and bind sediment grains are known to increase sediment cohesivity and sea floor stability (Murray et al., 2002; Malarkey et al., 2015; Craig et al., 2019). In particular, EPS acts to bind sediment together and counteract grain-size segregation (Malarkey et al., 2015). Furthermore, at the salinity levels observed in the present flow, EPS is shown to be a far more effective binding agent relative to clay in sand-rich sediments (Parsons et al., 2016).

The above feedbacks among flow dynamics, sediment type, geomorphology and benthic fauna suggest that near-bed flow is a primary control on sediment type, but it fails to explain the at-a-point distributions of sediment grain size and the limited nature of grain-size segregation. The ubiquitous presence of organisms and their products might therefore have feedback on the ability of the flow to move sediment around the bend.

5.1.3 | Benthic biology and sediment type

Organisms occupy different areas of the channel according to the sea floor sediment type, which is itself a function of flow velocity (Figure 8). Studies in the area have suggested this flow velocity is quasi-steady, which may explain the high density of organisms of a few species found in the channel (Connell, 1978). As noted above, benthic biology might have an important influence on sediment mobility by sediment trapping, binding, sediment cohesion and overall stabilisation of the sea floor (Murray et al., 2002; Tolhurst et al., 2002; Craig et al., 2019). This influence could well promote the observed broad sediment grain distribution and the lack of segregation of cohesive and non-cohesive sediment on the channel sea floor.

Recent papers have demonstrated that biological materials (e.g. EPS) can have a profound influence on sea floor sediment characteristics such as strength, roughness and porosity (Figure 8; Malarkey et al., 2015; Craig et al., 2019). This influence could vary significantly by system according to the organisms present. Organisms on the top layer of the sea floor may also physically protect sediment from suspension, representing a biological shield to flow (Murray et al., 2002), influence small-scale seabed roughness or generate low-velocity (<10 cm/s) siphonal currents with consequent impacts on the near-bed flow (Monismith et al., 1990). However, these small-scale effects are not considered in this study because any associated small-scale bedforms that result from such interactions are below the resolution of the bathymetric data used here (Malarkey et al., 2015).

In summary, the flow drives sediment transport and deposition, which in turn dictates the distribution of different organisms. However, sediment transport also causes changes to the morphology of the channel, that is the presence of bars within the channel. These morphological features, in turn, locally steer the flow and influence flow velocity. All these aspects are in keeping with a physically driven link between flow processes and sedimentation. However, the overall stability of the sediment bed is a function of the colonising biology, as, otherwise based purely on physical processes, the bed is predicted to be fully mobile. This biologically-induced stability is reflected in the sediment distributions, which are very broad and contain a high percentage of fines (<63 µm). This points to a close coupling of the benthic organisms and the sea floor sediments; molluscs are located in coarser-grained higher velocity sections, while the tube-living organisms establish themselves in finer-grained lower velocity zones. However, in both cases, they then produce feedback, acting to help protect the surface and to trap and bind finer-grained sediments. This coupling between sediment colonising fauna and the sediment will in turn greatly affect the ability of the flow to erode and transport sediment, probably accounting for the paradoxical relationship between the comparative sediment stability observed herein and the predicted bed mobility based solely on flow process estimates.

5.2 | Application to deep-sea submarine channels

The present study has examined the role of benthic biology on subaqueous channel sedimentary processes in shallow depths (70–80 m). However, subaqueous channels are known to be hotspots for benthic fauna at far greater depths; examples include the Cascadia Channel at ca 3 km depth (Griggs et al., 1969) and the Congo Channel at ca 4 to 5 km depth (Olu et al., 2017; Pozzato et al., 2017; Sen et al., 2017). Furthermore, subaqueous channels can be found in even the deepest parts of the ocean (McArthur & Tek, 2021). The nature of the benthic biology is known to change with depth (Watling et al., 2013), although there has been no study that has examined this specifically for submarine channels. Consequently, given the dearth of knowledge on the nature of benthic communities within deep-sea channels, it is hard to extrapolate the present results to deepwater. The present study, rather, demonstrates the principle that benthic organisms can be important controls on channel sedimentation, and given the known importance of deep-sea channels as biological hotspots, it is to be expected that this extends to deepwater systems. The

hope is that the present work will focus attention on the role of biotic controls on submarine channels, and that future work will examine the question of how such processes change as a function of water depth, alongside a range of other potential controls.

5.3 | Implications for interpreting the geological record

In this work, a modern system has been studied in order to understand the relationship between near-bed flow and sediment distribution in a sea floor channel bend and the influence of other often disregarded factors, such as benthic biology. An important application of this work is achieving better interpretations of palaeoflow characteristics from channel bend deposits preserved in the geological record. Studies of channel bends in the geological record have tended to focus on sediment grain sizes and small-scale sedimentary structures alone to infer flow character and velocity (Pyles et al., 2012; Jobe et al., 2016). An important result in this study is that while there is correlation between near-bed flow velocity and sediment type (gravel, sand and mud), there is poor correlation between near-bed flow velocity and grain size (e.g. d_{50}). Two reasons for this have been proposed. First, the presence of organisms, many of which will not be preserved in the geological record, can increase the stability and cohesivity of sea floor fine sediments. Second, there is added stability due to the mixed cohesive/non-cohesive sediments found on the sea floor as opposed to the single grain sizes used to create sediment mobility diagrams.

Evidence of biology (e.g. trace fossils) can be found in ancient channels (Cummings & Hodgson, 2011; Mángano et al., 2016). However, this record might be preservation-biased towards either hard-bodied organisms or certain types of soft-bodied organisms, rather than say the tube-living organisms in this study. As yet, the influence of life in ancient submarine channels has not been considered when interpreting ancient flow characteristics. This study highlights the need not only to develop interdisciplinary studies (such as sedimentology, flow dynamics and benthic biology) in modern and ancient systems but also to investigate variations in biological abundance in different submarine channel systems and through time in response to evolution and mass extinctions.

6 | CONCLUSIONS

This study shows, using a unique dataset that looks at spatial variations in physical and biological parameters around a bend, that biota can play a major role in

sedimentation within submarine channels and that, in turn, this will influence channel morphology and evolution. While little work has been undertaken on submarine channel benthic biology, they are known to be biological hotspots, and therefore it is to be expected that in active systems, submarine channel deposits will be widely affected by biota. It is therefore argued that the current assumption that submarine channels are essentially abiotic, controlled by purely physical processes, is incorrect.

ACKNOWLEDGEMENTS

The authors would like to thank Professor Martin Solan from the University of Southampton for his support on identification of species present in the collected samples. This project was funded by Natural Environment Research Council (NERC) grants NE/F020511/1, NE/F020120/1 and NE/F020279/1. We thank the crew of the RV Pelagia, the RV Bilim-2 and the RV Koca Piri Reis for their assistance with cruise planning and operation, and the Marine Autonomous and Robotic Systems (MARS) engineers from NERC National Marine Facilities for AUV operational support. Professors Ali Aksu and Rick Hiscott of Memorial University, Canada, Prof. Roger Flood of Stony Brook University, USA and Prof. Dogan Yasar of Dokuz Eylül University, Turkey, are thanked for their help with the 2010 field campaign. We thank the two anonymous reviewers and the Editor, Peter Swart, for their constructive comments, which helped improve the paper.

CONFLICT OF INTEREST STATEMENT

The authors have no conflicts of interest to declare. All co-authors have seen and agree with the contents of the manuscript, and there is no financial interest to report.

DATA AVAILABILITY STATEMENT

The data that support the findings of this study are available on <https://doi.org/10.5518/1357>.

ORCID

M. Azpiroz-Zabala  <https://orcid.org/0000-0003-1267-2384>

REFERENCES

- Aksu, A.E. & Hiscott, R.N. (2022) Persistent Holocene outflow from the Black Sea to the eastern Mediterranean Sea still contradicts the Noah's Flood Hypothesis: A review of 1997–2021 evidence and a regional paleoceanographic synthesis for the latest Pleistocene–Holocene. *Earth-Science Reviews*, 227, 103960.
- Amos, K.J., Peakall, J., Bradbury, P.W., Roberts, M., Keevil, G. & Gupta, S. (2010) The influence of bend amplitude and planform morphology on flow and sedimentation in submarine channels. *Marine and Petroleum Geology*, 27(7), 1431–1447. <https://doi.org/10.1016/j.marpetgeo.2010.05.004>

- Azpiroz-Zabala, M., Cartigny, M.J.B., Sumner, E.J., Clare, M.A., Talling, P.J., Parsons, D.R. & Cooper, C. (2017a) A general model for the helical structure of geophysical flows in channel bends. *Geophysical Research Letters*, 44, 11,932–11,941. <https://doi.org/10.1002/2017GL075721>
- Azpiroz-Zabala, M., Cartigny, M.J.B., Talling, P.J., Parsons, D.R., Sumner, E.J., Clare, M.A. & Pope, E.L. (2017b) Newly recognized turbidity current structure can explain prolonged flushing of submarine canyons. *Science Advances*, 3(10), e1700200. <https://doi.org/10.1126/sciadv.1700200>
- Babonneau, N., Savoye, B., Cremer, M. & Bez, M. (2010) Sedimentary architecture in meanders of a submarine channel: Detailed study of the present Congo turbidite channel (Zaiango Project). *Journal of Sedimentary Research*, 80(10), 852–866. <https://doi.org/10.2110/jsr.2010.078>
- Bolla Pittaluga, M. & Imran, J. (2014) A simple model for vertical profiles of velocity and suspended sediment concentration in straight and curved submarine channels. *Journal of Geophysical Research: Earth Surface*, 119, 483–503. doi:10.1002/2013JF002812
- Brandon, M. & Civitelli, G. (2007) Non-seagrass meadow sedimentary facies of the Pontinian Islands, Tyrrhenian Sea: A modern example of mixed carbonate-siliciclastic sedimentation. *Sedimentary Geology*, 201, 286–301.
- Clark, J.D. & Pickering, K.T. (1996) *Submarine channels: Processes and architecture*. London: Vallis Press, p. 231.
- Connell, J.H. (1978) Diversity in tropical rain forests and coral reefs. *Science*, 199(4335), 1302–1310. <https://doi.org/10.1126/science.199.4335.1302>
- Craig, M.J., Baas, J.H., Amos, K.J., Strachan, L.J., Manning, A.J., Paterson, D.M., Hope, J.A., Nodder, S.D. & Baker, M.L. (2019) Biomediation of submarine sediment gravity flow dynamics. *Geology*, 48, 72–76. <https://doi.org/10.1130/G46837.1>
- Cummings, J.P. & Hodgson, D.M. (2011) Assessing controls on the distribution of ichnotaxa in submarine fan environments, the Basque Basin, Northern Spain. *Sedimentary Geology*, 239(3–4), 162–187. <https://doi.org/10.1016/j.sedgeo.2011.06.009>
- Dorrell, R.M., Darby, S.E., Peakall, J., Sumner, E.J., Parsons, D.R. & Wynn, R.B. (2013) Superelevation and overspill control secondary flow dynamics in submarine channels. *Journal of Geophysical Research: Oceans*, 118, 3895–3915. <https://doi.org/10.1002/jgrc.20277>
- Dorrell, R.M., Peakall, J., Sumner, E.J., Parsons, D.R., Darby, S.E., Wynn, R.B., Özsoy, E. & Tezcan, D. (2016) Flow dynamics and mixing processes in hydraulic jump arrays: Implications for channel-lobe transition zones. *Marine Geology*, 381, 181–193. <https://doi.org/10.1016/j.margeo.2016.09.009>
- Dorrell, R.M., Amy, L.A., Peakall, J. & McCaffrey, W.D. (2018) Particle size distribution controls the threshold between net sediment erosion and deposition in suspended load dominated flows. *Geophysical Research Letters*, 45, 1443–1452.
- Fernandes, A.M., Buttles, J. & Mohrig, D. (2020) Flow substrate interactions in aggrading and degrading submarine channels. *Journal of Sedimentary Research*, 90(6), 573–583. <https://doi.org/10.2110/jsr.2020.31>
- Flood, R.D., Hiscott, R.N. & Aksu, A.E. (2009) Morphology and evolution of an anastomosed channel network where saline underflow enters the Black Sea. *Sedimentology*, 56, 807–839. <https://doi.org/10.1111/j.1365-3091.2008.00998.x>
- Frey, P.L., de Micheaux, H., Bel, C., Maurin, R., Rorsman, K., Martin, T. & Ducottet, C. (2020) Experiments on grain size segregation in bedload transport on a steep slope. *Advances in Water Resources*, 136, 103478.
- Gili, J.M., Bouillon, J., Page, F., Palanques, A. & Puig, P. (1999) Submarine canyons as habitats of prolific plankton populations: Three new deep-sea Hydroidomedusae in the western Mediterranean. *Zoological Journal of the Linnean Society*, 125, 313–329.
- Gregg, M.C. & Özsoy, E. (1999) Mixing on the Black Sea shelf North of the Bosphorus. *Geophysical Research Letters*, 26, 1869–1872.
- Gregg, M.C., Özsoy, E. & Latif, M.A. (1999) Quasi-steady exchange flow in the Bosphorus. *Geophysical Research Letters*, 26, 83–86.
- Griggs, S.B., Carey, A.G., Jr. & Kulm, L.D. (1969) Deep-sea sedimentation and sediment-fauna interaction in Cascadia Channel and on Cascadia Abyssal Plain. *Deep Sea Research*, 16, 157–170.
- Halfar, J., Ingle, J.C., Jr. & Godniz-Orta, L. (2004) Modern non-tropical mixed carbonate-siliciclastic sediments and environments of the southwestern Gulf of California, Mexico. *Sedimentary Geology*, 165, 93–115.
- Harris, P.T. & Whiteway, T. (2011) Global distribution of large submarine canyons: Geomorphic differences between active and passive continental margins. *Marine Geology*, 285, 69–86.
- Hiscott, R.N., Aksu, A.E., Flood, R.D., Kostylev, V. & Yaşar, D. (2013) Widespread overspill from a saline density-current channel and its interaction with topography on the south-west Black Sea shelf. *Sedimentology*, 60, 1639–1667. <https://doi.org/10.1111/sed.12071>
- Jobe, Z., Sylvester, Z.B., Pittaluga, M., Frascati, A., Pirmez, C., Minisini, D., Howes, N. & Cantelli, A. (2016) Facies architecture of submarine channel deposits on the western Niger Delta slope: Implications for grain-size and density stratification in turbidity currents. *Journal of Sedimentary Research*, 86, 73–86. <https://doi.org/10.2110/jsr.2016.3>
- Kane, I.A., McCaffrey, W.D. & Peakall, J. (2008) Controls on sinuosity evolution within submarine channels. *Geology*, 36(4), 287–290. <https://doi.org/10.1130/G24588A.1>
- Kane, I.A. & Clare, M.A. (2019) Dispersion, accumulation, and the ultimate fate of microplastics in deep-marine environments: a review and future directions. *Frontiers in earth science*, 7, 80.
- Kassem, A. & Imran, J. (2004) Three-dimensional modeling of density current. II. Flow in sinuous confined and unconfined channels. *Journal of Hydraulic Research*, 42(6), 591–602. <https://doi.org/10.1080/00221686.2004.9628313>
- Khripounoff, A., Vangriesheim, A., Babonneau, N., Crassous, P., Dennielou, B. & Savoye, B. (2003) Direct observation of intense turbidity current activity in the Zaire submarine valley at 4000 m water depth. *Marine Geology*, 194(3–4), 151–158. [https://doi.org/10.1016/s0025-3227\(02\)00677-1](https://doi.org/10.1016/s0025-3227(02)00677-1)
- Kolla, V., Posamentier, H.W. & Wood, L.J. (2007) Deep-water and fluvial sinuous channels: Characteristics, similarities and dissimilarities and modes of formation. *Marine and Petroleum Geology*, 24, 388–405. <https://doi.org/10.1016/j.marpetgeo.2007.01.007>
- Konsoer, K., Zinger, J. & Parker, G. (2013) Bankfull hydraulic geometry of submarine channels created by turbidity currents: Relations between bankfull channel characteristics and formative flow discharge. *Journal of Geophysical Research: Earth Surface*, 118, 216–228. <https://doi.org/10.1029/2012JF002422>

- Kuenen, P.H. (1953) Origin and classification of submarine canyons. *GSA Bulletin*, 64, 1295–1313.
- de Leeuw, J., Eggenhuisen, J.T. & Cartigny, M.J.B. (2016) Morphodynamics of submarine channel inception revealed by new experimental approach. *Nature Communications*, 7, 10886. <https://doi.org/10.1038/ncomms10886>
- Malarkey, J., Baas, J.H., Hope, J.A., Aspiden, R.J., Parsons, D.R., Peakall, J., Paterson, D.M., Schindler, R.J., Ye, L., Lichtman, I.D. & Bass, S.J. (2015) The pervasive role of biological cohesion in bedform development. *Nature communications*, 6(1), 6257.
- Mángano, M.G., Buatois, L.A., Wilson, M. & Droser, M. (2016) The great Ordovician biodiversification event. In: Mángano, M.G. & Buatois, L.A. (Eds.) *Dordrecht, The Trace-Fossil Record of Major Evolutionary Events: Volume 1: Precambrian and Paleozoic, Topics in Geobiology*, Vol. 39, pp. 127–156.
- McArthur, A.D. & Tek, D.E. (2021) Controls on the origin and evolution of deep-ocean trench-axial channels. *Geology*, 49, 883–888.
- Mietta, F., Chassagne, C., Manning, A.J. & Winterwerp, J.C. (2009) Influence of shear rate, organic matter content, pH and salinity on mud flocculation. *Ocean Dynamics*, 59, 751–763.
- Monismith, S.G., Koseff, J.R., Thompson, J.K., O'Riordan, C.A. & Nepf, H.M. (1990) A study of model bivalve siphonal currents. *Limnology and Oceanography*, 35(3), 680–696.
- Murray, J.M.H., Meadows, A. & Meadows, P.S. (2002) Biogeomorphological implications of microscale interactions between sediment geotechnics and marine benthos: A review. *Geomorphology*, 47, 15–30. [https://doi.org/10.1016/S0169-555X\(02\)00138-1](https://doi.org/10.1016/S0169-555X(02)00138-1)
- Ockelford, A. & Yager, E. (2020) The initiation of motion and formation of armour layers. In: *Treatise on Geomorphology*, Volume 6.1, 2022, pp. 176–199.
- Olu, K., Decker, C., Pastor, L., Caprais, J.-C., Khipounoff, A., Morineaux, M., Ain Baziz, M., Menot, L. & Rabouille, C. (2017) Cold-seep-like macrofaunal communities in organic- and sulphide-rich sediments of The Congo deep-sea fan. *Deep Sea Research Part II: Topical Studies in Oceanography*, 142, 180–196. <https://doi.org/10.1016/j.dsr2.2017.05.005>
- Özsoy, E., di Iorio, D., Gregg, M.C. & Backhaus, J.O. (2001) Mixing in the Bosphorus Strait and the Black Sea continental shelf: Observations and a model of the dense water outflow. *Journal of Marine Systems*, 31, 99–135.
- Paradis, S., Puig, P., Masqué, P., Juan-Díaz, X., Martín, J. & Palanques, A. (2017) Bottom-trawling along submarine canyons impacts deep sedimentary regimes. *Scientific reports*, 7(1), 43332.
- Parsons, D.R., Peakall, J., Aksu, A.E., Flood, R.D., Hiscott, R.N., Besiktepe, S. & Moulard, D. (2010) Gravity-driven flow in a submarine channel bend: Direct field evidence of helical flow reversal. *Geology*, 38, 1063–1066. <https://doi.org/10.1130/G31121.1>
- Parsons, D.R., Jackson, P.R., Czuba, J.A., Engel, F.L., Rhoads, B.L., Oberg, K.A., Best, J.L., Mueller, D.S., Johnson, K.K. & Riley, J.D. (2013) Velocity Mapping Toolbox (VMT): A processing and visualization suite for moving-vessel ADCP measurements. *Earth Surface Processes and Landforms*, 38, 1244–1260. <https://doi.org/10.1002/esp.3367>
- Parsons, D.R., Schindler, R.J., Hope, J.A., Malarkey, J., Baas, J.H., Peakall, J., Manning, A.J., Ye, L., Simmons, S., Paterson, D.M., Aspiden, R.J., Bass, S.J., Davies, A.G., Lichtman, I.D. & Thorne, P.D. (2016) The role of biophysical cohesion on subaqueous bed form size. *Geophysical Research Letters*, 43, 1566–1573.
- Peakall, J., Kane, I.A., Masson, D.G., Keevil, G., McCaffrey, W. & Corney, R. (2012) Global (latitudinal) variation in submarine channel sinuosity. *Geology*, 40(1), 11–14. <https://doi.org/10.1130/g32295.1>
- Peakall, J., Darby, S.E., Dorrell, R.M., Parsons, D.R., Sumner, E.J. & Wynn, R.B. (2014) Comment on “A simple model for vertical profiles of velocity and suspended sediment concentration in straight and curved submarine channels” by M. Bolla Pittaluga and J. Imran. *Journal of Geophysical Research: Earth Surface*, 119(9), 2070–2073. <https://doi.org/10.1002/2014JF003211>
- Peakall, J. & Sumner, E.J. (2015) Submarine channel flow processes and deposits: A process-product perspective. *Geomorphology*, 244, 95–120. <https://doi.org/10.1016/j.geomorph.2015.03.005>
- Phillips, S. (1987) Dipmeter interpretation of turbidite-channel reservoir sandstones, Indian Draw field, New Mexico. In: Tillman, R.W. & Weber, K.J. (Eds.) *Reservoir sedimentology*, Vol. 40. *Society of Economic Paleontologists and Mineralogists. Special Publication*. Tulsa, Oklahoma, USA, pp. 113–128.
- Pirmez, C. & Imran, J. (2003) Reconstruction of turbidity currents in Amazon Channel. *Marine and Petroleum Geology*, 20, 823–849. <https://doi.org/10.1016/j.marpetgeo.2003.03.005>
- Pozzato, L., Cathalot, C., Berrached, C., Toussaint, F., Stetten, E., Caprais, J.-C. & Rabouille, C. (2017) Early diagenesis in The Congo deep-sea fan sediments dominated by massive terrigenous deposits: Part I – Oxygen consumption and organic carbon mineralization using a micro-electrode approach. *Deep Sea Research Part II: Topical Studies in Oceanography*, 142, 125–138. <https://doi.org/10.1016/j.dsr2.2017.05.010>
- Pyles, D.R., Tomasso, M. & Jennette, D.C. (2012) Flow processes and sedimentation associated with erosion and filling of sinuous submarine channels. *Geology*, 40(2), 143–146. <https://doi.org/10.1130/G32740.1>
- Sen, A., Dennielou, B., Tourole, J., Arnaubec, A., Rabouille, C. & Olu, K. (2017) (2017) Fauna and habitat types driven by turbidity currents in the lobe complex of the Congo deep-sea fan. *Deep-Sea Research Part II*, 142, 167–179.
- Simmons, S.M., Azpiroz-Zabala, M., Cartigny, M.J.B., Clare, M.A., Cooper, C., Parsons, D.R. et al. (2020) Novel acoustic method provides first detailed measurements of sediment concentration structure within submarine turbidity currents. *Journal of Geophysical Research: Oceans*, 125, e2019JC015904. <https://doi.org/10.1029/2019JC015904>
- Stefanescu, C., Morales-Nin, B. & Massuti, E. (1994) Fish assemblages on the slope in the Catalan Sea (western Mediterranean): Influence of a submarine canyon. *Journal of the Marine Biological Association of the United Kingdom*, 74(3), 499–512. <https://doi.org/10.1017/s0025315400047627>
- Sumner, E.J., Peakall, J., Parsons, D.R., Wynn, R.B., Darby, S.E., Dorrell, R.M., McPhail, S.D., Perrett, J., Webb, A. & White, D. (2013) (2013) First direct measurements of hydraulic jumps in an active submarine density current. *Geophysical Research Letters*, 40, 5904–5908. <https://doi.org/10.1002/2013GL057862>
- Sumner, E.J., Peakall, J., Dorrell, R.M., Parsons, D.R., Darby, S.E., Wynn, R.B., McPhail, S.D., Perrett, J., Webb, A. & White, D. (2014) Driven around the bend: Spatial evolution and controls on the orientation of helical bend flow in a natural submarine

- gravity current. *Journal of Geophysical Research: Oceans*, 119, 898–913. doi:[10.1002/2013JC009008](https://doi.org/10.1002/2013JC009008)
- Szupiany, R.N., Amsler, M.L., Best, J.L. & Parsons, D.R. (2007) Comparison of fixed- and moving vessel measurements with an aDp in a large river. *Journal of Hydraulic Engineering*, 133, 1299–1309. [https://doi.org/10.1061/\(ASCE\)0733-9429\(2007\)](https://doi.org/10.1061/(ASCE)0733-9429(2007)0733-9429)
- Talling, P.J., Paull, C.K. & Piper, D.J.W. (2013) How are subaqueous sediment density flows triggered, what is their internal structure and how does it evolve? Direct observations from monitoring of active flows. *Earth-Science Reviews*, 125, 244–287. <https://doi.org/10.1016/j.earscirev.2013.07.005>
- Tolhurst, T.J., Gust, G. & Paterson, D.M. (2002) The influence of an extracellular polymeric substance (EPS) on cohesive sediment stability. In: Winterwerp, J.C. & Kranenburg, C. (Eds.) *Fine sediment dynamics in the marine environment*. Amsterdam: Elsevier, pp. 409–425. 1st Edition, Volume 5-June 5.
- UNESCO. (1983) Algorithms for computation of fundamental properties of seawater, UNESCO Tech. Pap. in Mar. Sci. 44, 53 pp., UNESCO Div. Mar. Sci., Paris.
- Ünlülata, Ü., Oğuz, T., Latif, M.A. & Özsoy, E. (1990) On the physical oceanography of the Turkish Straits. In: Pratt, L.J. (Ed.) *The Physical Oceanography of Sea Straits*. NATO ASI Series, Vol. 318. Dordrecht: Springer, pp. 25–60. https://doi.org/10.1007/978-94-009-0677-8_2
- Walker, R.G. & Mutti, E. (1973) Turbidite facies and facies associations. In: Middleton, G.V. & Bouma, A.H. (Eds.) *Turbidites and deep water sedimentation: Pacific Section*. Los Angeles Short Course Notes: Society of Economic Paleontologists and Mineralogists, pp. 119–157.
- Watling, L., Guinotte, J., Clark, M.R. & Smith, C.R. (2013) A proposed biogeography of the deep ocean floor. *Progress in Oceanography*, 111, 91–112.
- Wei, T., Peakall, J., Parsons, D.R., Chen, Z., Zhao, B. & Best, J. (2013) Three-dimensional gravity current flow within a subaqueous bend: Spatial evolution and force balance variations. *Sedimentology*, 60, 1668–1680.
- Wells, M.G. & Dorrell, R.M. (2021) Turbulence processes within turbidity currents. *Annual Review of Fluid Mechanics*, 53, 59–83. <https://doi.org/10.1146/annurev-fluid-010719-060309>
- Wynn, R.B., Cronin, B.T. & Peakall, J. (2007) Sinuous deep-water channels: Genesis, geometry and architecture. *Marine and Petroleum Geology*, 24, 341–387.
- Yu, G. & Tan, S.-K. (2006) Errors in the bed shear stress as estimated from vertical velocity profile. *Journal of Irrigation and Drainage Engineering*, 132, 490–497. [https://doi.org/10.1061/\(ASCE\)0733-9437\(2006\)132:5\(490\)](https://doi.org/10.1061/(ASCE)0733-9437(2006)132:5(490))

SUPPORTING INFORMATION

Additional supporting information can be found online in the Supporting Information section at the end of this article.

How to cite this article: Azpiroz-Zabala, M., Sumner, E.J., Cartigny, M.J.B., Peakall, J., Clare, M., Darby, S.E. et al. (2024) Benthic biology influences sedimentation in submarine channel bends: Coupling of biology, sedimentation and flow. *The Depositional Record*, 00, 1–17. Available from: <https://doi.org/10.1002/dep2.265>